Journal of Materials Chemistry B

Accepted Manuscript

ROYAL SOCIETY OF CHEMISTRY

www.rsc.org/materialsB

Peptide Nanofiber-$CaCO_3$ Composite Microparticles as Adjuvant-free Oral Vaccine Delivery Vehicles

Joshua D. Snook[1#], Charles B. Chesson[2,3#], Alex G. Peniche[4], Sara M. Dann[2,4], Adriana Paulucci[5], Iryna V. Pinchuk[2,6], and Jai S. Rudra[1,3*]

[1]Department of Pharmacology & Toxicology, [2]Institute for Translation Sciences, [3]Sealy Center for Vaccine Development, [4]Department of Internal Medicine-Division of Infectious Diseases, [6]Department of Internal Medicine-Division of Gastroenterology, University of Texas Medical Branch, Galveston, TX 77555

[5]University of Texas MD Anderson Cancer Center, Houston TX 77030

# equal contribution first authors

[*]Corresponding author

Jai S. Rudra, Assistant Professor
Department of Pharmacology and Toxicology
Sealy Center for Vaccine Development
Basic Sciences Building 3.308, Route 0617
301 University Blvd, Galveston, TX 77555
P: 409 772 9649 F: 409 772 9648
E: jarudra@utmb.edu

ABSTRACT

To combat mucosal pathogens that cause gastrointestinal (GI) infections, local mucosal immunity is required which is best achieved through oral vaccination. Oral delivery of vaccines is also a safe and convenient alternative to injected vaccines due to its non-invasive nature and high compliance rate for all ages. However, the lack of effective and safe mucosal adjuvants, the selective permeability of the mucus barrier, and the harsh GI environment continue to pose a significant challenge for oral vaccine development. Microparticle-based strategies are attractive for oral vaccination due to their ability to efficiently penetrate the mucus barrier and have the added advantage of protecting the antigen in the harsh gastric environment. In this work, self-adjuvanting peptide nanofiber-$CaCO_3$ composite microparticles were prepared and investigated for oral vaccine delivery. Compared to polymeric microparticles, inorganic $CaCO_3$ microparticles have unique advantages due to the biocompatibility of $CaCO_3$ as a natural mineral, mild preparation conditions, and its porous structure that is suitable for loading other materials. Particle size distribution, nanofiber loading efficiency, morphology, and degradation in simulated gastric fluid were characterized. The composite microparticles were efficient at penetrating the mucus barrier and were localized to immune inductive sites and elicited the production of mucosal antibody responses, particularly the protective IgA isotype following oral administration. The magnitude of the mucosal immune response was comparable to the gold-standard adjuvant cholera toxin B (CTB). Our results indicate that OVA-KFE8/$CaCO_3$ composite microparticles are efficient self-adjuvanting oral vaccine delivery vehicles for induction of mucosal antibody responses.

Key Words: calcium carbonate, composite microparticle, oral vaccination, peyer's patches, peptide nanofibers, self-assembly

INTRODUCTION

It is estimated that 70% of human pathogens initiate infection via the mucosal surfaces and the intestinal mucosa is especially vulnerable to infections caused by bacteria, viruses, and protozoa[1]. Injected vaccines are often very poor at inducing mucosal immunity and local immunity in the gut is best induced by oral vaccination, which has the added advantage of being a needle and medical-waste free strategy[2]. The WHO estimates that unsafe healthcare injections accounted for 5% of HIV, 32% of hepatitis B and 40% of hepatitis C infections acquired in developing countries making oral vaccination a highly attractive alternative[3]. Oral vaccination also stimulates productive immune responses at distal sites via the interconnected mucosa-associated lymphoid tissue (MALT) and offers an avenue for mass vaccination programs in developing countries with high patient compliance, eliminating the need for skilled personnel, and limiting the risk of infections due to needle reuse and medical waste[4,5].

Currently, approved oral vaccines are based on inactivated or attenuated pathogens, which in general suffer from poor safety profiles and maintain a risk of reversion to virulence[6]. Subunit vaccines based on purified or recombinant peptide/protein antigens are safer, however they are poorly immunogenic and need to be co-administered with adjuvants for enhancing antibody and cellular immune responses[7,8]. In the U.S. only alum-based adjuvants are licensed for clinical use and limited to parenteral route of administration[9]. Bacterial toxins, such as cholera toxin (CT) and the heat-labile enterotoxin (LT) of *Escherichia coli* are the most potent and extensively studied mucosal adjuvants available, but they are too toxic for clinical use[10-12]. Additionally, the highly acidic and protease-rich environment of the gastrointestinal (GI) tract poses a significant barrier to the integrity and effective translocation of vaccines across the gut mucosa associated lymphoid tissues (GALT also known as MALT) [5,13]. GALT consists of the

diffuse lymphoid tissue such as lamina propria and organized lymphoid tissue, which includes Peyers patches (PP) and isolated lymphoid follicles[1,14]. At the sites of organized MALT, antigens are taken up by M cells, which are involved in the initiation of acquired antigen-specific immune responses, such as IgA induction, via the uptake of luminal antigens[15]. M cells specialize in taking up antigen from the intestinal lumen and translocate it to GALT where DCs present it to the B cells and T cells leading to production of strong and protective IgA responses[15,16]. Therefore, oral vaccination strategies that are self-adjuvanting and efficiently translocate antigens across the mucus barrier to immune inductive sites are highly desirable.

Polymeric micro/nano particle-based strategies are attractive for oral vaccination due to their ability to efficiently penetrate the mucus barrier and have the added advantage of protecting the antigen in the harsh gastric environment[1,17,18]. Oral vaccine delivery systems based on poly(lactide-co-glycolic acid) (PLGA) microparticles[19], enteric coating polymers[20], chitosan microspheres[21,22], yeast β-glucan microparticles[23], and cationic liposomes[24] have been successfully developed and tested in small animal models. However, the widely adopted production-scale methodologies for fabrication of polymeric micro- and nanoparticles involve the use of organic solvents and cross-linkers, even low levels of exposure to which, could lead to toxic side effects[25]. Also, inclusion of exogenous adjuvants and surface modification strategies are required to enhance the potency and penetration of the polymeric particles across the mucus barrier[4,14]. To date only formulations based on PLGA and liposomes have progressed from animal models to clinical trials[26].

We previously reported an adjuvant-free vaccination platform based on self-assembling, β-sheet rich, peptide nanofibers, which induce robust humoral and cellular immune responses when linked to peptide or protein antigens[27-31]. Parenteral vaccination with peptide nanofibers

has been shown to elicit protective immune responses in mouse models of malaria[29], cancer[32], and influenza[30]. However, the microenvironment and cellular populations of GALT differ significantly from peripheral lymph nodes and are therefore distinct as an inductive site for priming of acquired immune responses[1]. Therefore the adjuvanting ability of self-assembling peptide nanofibers when delivered orally needs to be defined. Also, based on our current understanding of mucosal immunology, particulate antigens are highly effective at inducing mucosal immunity compared to soluble antigens and encapsulation strategies that render soluble nanofibers into particulate form would enhance their translocation across the mucus barrier and also protect them from the harsh GI environment[5].

Here, we report peptide nanofiber-$CaCO_3$ composite microparticles as self-adjuvanting oral vaccine delivery vehicles. Compared to polymeric microparticles, inorganic $CaCO_3$-microparticles have unique advantages such as preparation in mild physiological buffers, biocompatibility, and biodegradability[33,34]. We synthesized peptide nanofiber-$CaCO_3$ composite microparticles by precipitating $CaCO_3$ in aqueous buffers containing self-assembling peptide nanofibers bearing the model antigenic peptide OVA (chicken egg ovalbumin 323-339). The loading efficiency, size distribution, and morphology of the composite microparticles was characterized and their uptake by antigen-presenting cells (APCs) was investigated using in vitro bone marrow derived dendritic cell cultures (BMDCs). Phagocytosis of composite microparticles by antigen-presenting cells (APCs) in the GALT was investigated using ligated ileal loop assays. The production of mucosal and systemic antibody responses following oral administration of composite microparticles was investigated in mice. Our results indicate peptide nanofiber-$CaCO_3$ composite microparticles are effective as self-adjuvanting oral vaccine delivery vehicles for efficient induction of mucosal and systemic immune responses.

RESULTS & DISCUSSION

OVA-KFE8/$CaCO_3$ composite microparticle synthesis and characterization

Successful synthesis of OVA-KFE8/$CaCO_3$ composite microparticles was achieved by dissolving OVA-KFE8 nanofibers in 0.33 M $CaCl_2$ and an equal volume of 0.33 M Na_2CO_3 was added under stirring[35]. Precipitation of $CaCO_3$ microparticles in the presence of OVA-KFE8 nanofibers led to the encapsulation of the nanofibers in the microparticle core (Fig. 1a). For visualization purposes rhodamine-OVA-KFE8 nanofibers were used. Confocal imaging of labeled nanofibers indicated gelatinous random aggregates, which were transformed into discrete fluorescent microparticles after precipitation, indicating loading of the fluorescent nanofiber within the $CaCO_3$ matrix (Fig. 1b).

The loading efficiency and morphology of the composite microparticles was found to be dependent on the concentration of nanofiber stock solution. Highest loading efficiency of ~72% was achieved when microparticles were synthesized using a 2 mM solution of OVA-KFE8 nanofibers (Fig. 2a). At higher concentrations OVA-KFE8 nanofibers formed viscous solutions, which prevented optimal stirring. To assess whether the nanofibers were uniformly distributed within the microparticle or were mostly surface bound, microparticles loaded with rhodamine-OVA-KFE8 nanofibers were washed in PBS, and leaching of the nanofibers was measured by fluorescence spectroscopy. To calculate percentage of loaded nanofibers released during serial washes, microparticles were dissolved in 0.5 M ethylenediaminetetraacetic acid (EDTA) leading to 100% release of the nanofibers[36]. Data indicated that only ~8% of the nanofibers leached out after the first wash and significantly decreased over serial washes and after 5 wash cycles ~15%

of the OVA-KFE8 nanofibers were lost while ~85% were encapsulated within the $CaCO_3$ core (Fig. 2b) indicating that the bulk of the nanofibers were retained within the microparticles.

Scanning electron microscopy revealed highly spherical structures and while subtle differences in surface morphology were evident between pure $CaCO_3$ and OVA-KFE8/$CaCO_3$ composite microparticles (Fig. 3a and 3b), gross differences in cross-sectional morphology were observed. Control microparticles had a highly porous interior (Fig. 3a) while the composite particles were dense and devoid of any porosity suggesting encapsulation of the nanofibers within the microparticle core (Fig. 3b). Mean diameter of control microparticles was found to be 3.5 μm (Fig. 3c), whereas the composite microparticles had an average diameter of 2.2 μm (Fig. 3d), which is ideal for phagocytosis by APCs such as dendritic cells (DCs) and macrophages. Composite microparticles were also found to have a tighter size distribution profile compared to controls (Fig. 3d). The microparticles of $CaCO_3$ were formed by precipitation reaction between calcium chloride and sodium carbonate and the growing calcium carbonate cores captured nanofibers within them. Previous reports have suggested that presence of additives such as proteins and polymers may affect the crystallization process[37]. This has been attributed to increased viscosity of the reaction mixture leading to reduced ion diffusion rates, which slows down crystallization and causes a general decrease in particle size. While globular proteins like BSA do not significantly affect particle size, long chain polymers like ethylene glycol affect particle size in a concentration-dependent fashion[38]. The peptide nanofibers are long polymeric aggregates and presumably shift the particle formation process from crystal growth to oriented attachment of primary nanoparticles, which could possibly be the reason for smaller size of the composite microparticles. In summary, our data suggest that OVA-KFE8/$CaCO_3$ composite

microparticles can be synthesized under mild physiological conditions with high yields and tight control over particle morphology and size distribution.

Stability of composite microparticles in acidic environment

To determine the likelihood of OVA-KFE8/$CaCO_3$ composite microparticles surviving the highly acidic gastric environment without loss of encapsulated nanofiber cargo, the degradation of $CaCO_3$ and release of rhodamine-OVA-KFE8 nanofibers was measured using simulated gastric fluid (SGF)[39]. Microparticles were treated with 0.5 M EDTA (100% release) or PBS (no release) to calculate the percentage of nanofibers released following incubation in SGF (pH 1.2). To determine the nature of microparticle degradation, composite microparticles incubated for 90 min in SGF were visualized using scanning electron microscopy. Data indicated that the microparticles retained their spherical morphology similar to controls (Fig. 4a) but displayed increased porosity suggesting that they underwent surface degradation (Fig. 4b). Fluorescence intensity measurements indicated that 12% of the encapsulated nanofibers were released within the first 5 min and increased to 15% after 30 min (Fig. 4c). The nanofiber release plateaued over the next 60 min and at the end of 90 min of incubation ~20% of the encapsulated nanofibers fibers were released (Fig. 4c). The composite microparticles retained their spherical morphology and ~80% of encapsulated nanofibers after 90 min of incubation in SGF suggesting that they can be useful as oral antigen delivery vehicles.

Uptake of composite microparticles by BMDCs *in vitro*

Previous studies have demonstrated that peptide nanofibers are actively phagocytized by DCs and macrophages when injected into mice. Interestingly, only DCs exhibited increased

expression of B7 co-stimulatory molecules CD80 and CD86 after nanofiber uptake while expression of these molecules by macrophages remained unchanged[40]. These molecules are critical for the induction of T cell proliferation/activity in response to the antigen presentation by APCs[39]. Therefore, we examined whether OVA-KFE8/$CaCO_3$ composite microparticles could activate dendritic cells *in vitro*. To this end, BMDCs were incubated with composite microparticles and up-regulation of maturation markers CD80 and CD86 was determined using flow cytometry. Untreated or BMDCs incubated with OVA-KFE8 nanofibers were used as controls. Data indicated higher levels of CD80 and CD86 expression by BMDCs incubated in the presence of composite microparticles compared to OVA-KFE8 nanofibers or controls (Fig. 5a and 5b). Also, BMDCs incubated with OVA-KFE8 nanofibers had higher levels of CD80, and to a lesser extent CD86, compared to controls (Fig. 5a and 5b). Confocal microscopy indicated that OVA-KFE8/$CaCO_3$ composite microparticles were efficiently phagocytized by BMDCs and had stellate morphology suggesting maturation (Fig. 5c).

Innate immune responses elicited by APCs in response to the stimulation of toll-like and nod-like pattern recognition receptor activation are critical for the chemo-attraction and regulation of effector immune responses[42]. It is not known whether self-assembling peptide nanofibers or inorganic minerals such as $CaCO_3$ are capable of activating those innate immune receptors on APCs. However, particulates such as silica, asbestos, and aluminum salts have been shown to activate the NLRP3 inflammasome pathway leading to the production of the cytokine IL-1β, which supports the recruitment of pro-inflammatory immune cells. ELISA data indicated significantly higher levels of IL-1β in cultures of BMDCs treated with composite microparticles compared to OVA-KFE8 nanofibers or controls (Fig 5D). Although production of IL-1β is not direct evidence of NLRP3 inflammasome activation, the data suggest that OVA-KFE8/$CaCO_3$

composite microparticles, while improving the delivery of antigens to DCs, can also stimulate DCs to produce IL-1β, which is involved in the recruitment of the effector cells and induction of Th17 response, critical to the clearance of several mucosal pathogens[43,44].

Mechanisms of composite microparticle sampling *in vivo*

The harsh environment in the intestinal mucosa and the mucus coating provide a strong barrier not only for pathogen entry but also vaccine delivery[5]. A prerequisite for an efficient oral vaccine is to be able to efficiently translocate across the mucus barrier and be taken up by GALT where it will be efficiently presented by APCs to T and B cells to elicit protective immune responses[45]. The most well studied mechanisms of antigen sampling in the gut are uptake by M cells present in the follicle-associated epithelium, located just above the PPs, in which $CCR6^+$ DC will present antigens sampled by M cells to T cells[46]. Other mechanisms include $CX3CR1^+$ APCs that populate the mucosal lamina propria of the small intestine, which depend on the chemokine receptor CX3CR1 to form transepithelial dendrites to directly sample luminal antigens[47]. To determine whether uptake of OVA-KFE8/$CaCO_3$ composite microparticles occurred *in vivo* and if M cell and/or $CX3CR1^+$ APCs uptake mechanisms were involved, ligated intestinal ileal loop experiments were performed using transgenic $CX3CR1^{gfp/gfp}$ mice. Using rhodamine-OVA-FKE8 loaded microparticles and confocal microscopy it was observed that the composite microparticles translocated across the lumen and were co-localized with $CX3CR1^+$ APCs in the lamina propria (Fig 6A). Anti-M cell antibodies were used to determine efficiency of the composite microparticles uptake by M cells in these experiments. We observed that composite microparticles were co-localized with M cells suggesting translocation of the composite microparticles also occurs through M cells (Fig 6B).

Previous studies have demonstrated a key role for mesenteric lymph nodes (MLNs) as an inductive site in PP-deficient mice and that the intestinal lamina propria–MLN axis performs a potent mucosal inductive function in addition to the PPs[4,48]. Therefore to assess whether mesenteric lymph nodes were a major site for the drainage of composite microparticles, $CX3CR1^{gfp/gfp}$ mice were orally gavaged with rhodamine-OVA-KFE8 loaded composite microparticles and mesenteric lymph nodes collected after 2 h. Using confocal microscopy it was observed that $CX3CR1^{+}$ APCs that acquired the composite microparticles were found in MLN suggesting that APCs that acquire the composite microparticles from gut lumen and/or mucosal lamina propria migrate to MLN. Therefore, MLNs could be an active induction sites of mucosal antibody responses detected after vaccination with composite microparticles (Fig 6C). These findings indicate that OVA-KFE8/$CaCO_3$ composite microparticles are sampled by mechanisms involving $CX3CR1^{+}$ APCs in the lamina propria and M cells for presentation to B cells and T cells in the PP's, lymphoid follicles and MLNs.

Oral vaccination with OVA-KFE8/$CaCO_3$ composite microparticles

Given the favorable physicochemical and immunological characteristics of OVA-KFE8/$CaCO_3$ composite microparticles, we investigated their ability to induce mucosal antibody responses following oral administration in mice. Mice were vaccinated according to the schedule shown in Fig. 7a and control mice received PBS, OVA-KFE8 nanofibers, or OVA admixed with CTB. The concentration of all formulations was adjusted to ensure that all groups received equivalent amounts of OVA. Production of anti-OVA antibodies in the gut mucosa was measured using fecal extracts from the colon and systemic antibody responses were evaluated using sera. Using ELISA, significantly higher levels of antibodies (total IgG (H+L)) were detected in fecal extracts of mice vaccinated with OVA-KFE8/$CaCO_3$ composite microparticles

compared to mice vaccinated with OVA-CTB, OVA-KFE8 nanofibers, or PBS (Fig. 7b). Interestingly, it was observed that peptide nanofibers alone were also efficient at inducing adjuvant-free mucosal antibody responses when delivered orally, however their encapsulation in $CaCO_3$ microparticles significantly enhances the magnitude of the antibody response (Fig. 7b). This is presumably, due to efficient penetration of the particulates across the mucus barrier and enhanced uptake by gut-resident antigen-presenting cells. Our most interesting finding in the oral gavage studies is the significantly higher levels of antibodies in mice vaccinated with the composite microparticles compared to OVA-CTB (Fig. 7b). Evaluation of systemic antibody responses in the sera revealed only a few responders across all groups nonetheless antibody responses in mice vaccinated with composite microparticles were significantly higher than PBS or OVA-KFE8 nanofiber groups (Fig. 7c).

Antibody isotype IgA plays an important role in the protection of gastrointestinal, respiratory, and urogenital mucosal surfaces by regulating the symbiotic relationship existing between commensals and the host and preventing opportunistic infections[49]. Therefore fecal extracts were assayed using isotype specific IgG1, IgG2a, IgG2b, IgG3, IgM, and IgA primary antibodies. ELISA data showed significantly higher levels of IgA in mice vaccinated with OVA-KFE8/$CaCO_3$ composite microparticles compared to mice receiving PBS, OVA-KFE8 nanofibers, or OVA-CTB (Fig. 8a). Antibody isotype IgG1 was found to be significantly higher in the OVA-CTB group compared to all other groups (Fig. 8b). Also detectable and significantly higher levels of isotype IgG3 (Fig. 8c) and IgM (Fig. 8d) were observed in all groups compared to PBS. Levels of isotypes IgG2a and IgG2b were not detectable (below background levels). Based on these findings we conclude that OVA-KFE8/$CaCO_3$ composite microparticles are effective at inducing strong mucosal antibody responses when administered orally. In summary,

we have demonstrated that peptide-nanofiber/$CaCO_3$ composite microparticles are efficient self-adjuvanting oral vaccine delivery vehicles.

Our findings indicate that the working mechanism of the nanofiber-$CaCO_3$ composite microparticles is via enhanced uptake by DCs that sample the gut lumen and non-specific transcytosis through M cells. In this study, no exogenous adjuvants were incorporated into the composite microparticles to elicit antibody responses equivalent to those induced by CTB, a strong gold-standard mucosal adjuvant. While mucosal vaccination elicits both systemic and local immunity, the antigen doses required to elicit an immune response through the oral route are substantially higher. Encapsulation of the nanofibers into $CaCO_3$ microparticles not only protects the nanofibers in the harsh gastric environment but also ensures efficient delivery and antigen dose sparing for oral delivery. Studies using synthetic carriers for mucosal vaccination have demonstrated that particles with hydrophobic or net positive surface charge are mucoadhesive due to interactions with the negatively charged mucus layer[50]. Surface functionalization of hydrophobic PLGA microparticles with polyethylene glycol (PEG) chains has been shown to enhance their mucus penetrating properties[51]. $CaCO_3$ microparticles are intrinsically hydrophilic with a net neutral charge, which could enhance their translocation across the mucus barrier without further modification. Furthermore, they can be surface modified via simple adsorption with ligands specifically targeting receptors on antigen-presenting cells or M cells for targeted vaccine delivery.

We recently demonstrated that linking D amino acid self-assembling domains to antigens could enhance the potency of peptide nanofiber vaccines in mouse models[52]. This strategy can be used to improve the mucosal and antibody responses elicited by the composite microparticles through encapsulation of peptide nanofibers bearing an all-D amino acid self-assembling domain.

The chemical versatility of self-assembling peptide nanofibers allows for covalent linkage of whole protein antigens and recent studies demonstrated that protein-bearing self-assembling peptide nanofibers are self-adjuvanting[31]. This enables the development of composite microparticles loaded with protein-bearing nanofibers for enhancing the breath of protection and also covers broad population distributions. Furthermore, by controlling physical parameters such as agitation rate, mixing time, ionic strength, and temperature, $CaCO_3$ particle size and morphology can be controlled[53]. This allows for investigating the role of particle size and morphology on the uptake and sampling of microparticles in the GALT and the associated mucosal immune responses. Future embodiments of the current work will investigate, surface functionalization of the composite microparticles for targeted delivery to M cells, their ability to induce T helper cell responses with the appropriate immunological bias, and protect against challenge with mucosal pathogens.

Conclusions

In conclusion, this study demonstrates the feasibility of peptide nanofiber-$CaCO_3$ composite microparticles as oral vaccine delivery vehicles using the model antigen OVA. We show that composite microparticles can be synthesized under mild physiological conditions with tight size distribution profile, spherical morphology, and high nanofiber loading efficiency. The composite microparticles are able to withstand harsh acidic environment without significant loss of cargo or morphology and are phagocytized by antigen presenting cells *in vitro* leading to the production of pro-inflammatory cytokines. *In vivo*, the microparticles translocate across the mucus barrier and are sampled via classical antigen presenting mechanisms in the gut-associated lymphoid tissue. Oral vaccination with peptide nanofiber-$CaCO_3$ composite microparticles leads to the

production of robust mucosal antibody responses with appropriate isotypes advantageous for mucosal immunity.

EXPERIMENTAL

Synthesis of peptides and OVA-KFE8/$CaCO_3$ composite microparticles

Peptide nanofibers bearing the model antigenic peptide OVA were synthesized by coupling OVA (ISQAVHAAHAEINEAGR) to the N-terminus of the self-assembling peptide domain KFE8 (FKFEFKFE) via an amino acid linker (SGSG) using standard Fmoc Chemistry on a CS Bio-CS336X solid phase peptide synthesizer (CS Bio, CA). Rink Amide MBHA resin (Novabiochem, MA) was swelled in dry DMF for 1 h, and amino acids were double coupled using HBTU (O-(Benzotriazol-1-yl)-N,N,N′,N′-tetramethyluronium hexafluorophosphate) and HOBt (1-Hydroxybenzotriazole) chemistries. Peptides were cleaved from the resin using a 95% TFA/2.5% water/2.5% triisopropyl silane cocktail and precipitated in cold diethyl ether. The crude product was washed and purified by reverse-phase HPLC (C18 column) using Acetonitrile/H_2O gradients (>90% purity) and peptide mass was confirmed by MALDI-TOF mass spectrometry using α-cyano-4-hydroxycinnamic acid matrix (Bruker Daltonics, MA). All peptides were lyophilized and stored at -20 °C prior to use. OVA-KFE8/$CaCO_3$ composite microparticles were synthesized by colloidal crystallization technique reported previously[34]. Briefly, OVA-KFE8 nanofibers were prepared by dissolving the peptide in sterile water (8 mM stock solution), stored overnight at 4°C, and diluted to working concentration of 2 mM using 0.33 M sterile calcium chloride ($CaCl_2$). An equal volume of 0.33 M Na_2CO_3 was added under stirring (1000 rpm) and the mixture was stirred for additional 30 sec. The solution was allowed to stand for 30 min at RT and the precipitated OVA-KFE8/$CaCO_3$ composite microparticles

were obtained by centrifugation at 4000 rpm for 5 min. The particles were washed three times with DI water and dried under vacuum. For some studies composite microparticles were prepared using rhodamine-OVA-KFE8 nanofibers.

Loading efficiency, size distribution, and release studies

Loading efficiency of OVA-KFE8 nanofibers into $CaCO_3$ microparticles was calculated by the measuring the fluorescent intensity of a solution of rhodamine-conjugated OVA-KFE8 nanofibers (stock) before microparticle synthesis against the fluorescent intensity of the supernatant (sup) after microparticle synthesis. The loading efficiency was evaluated as follows:

$$Le = \frac{Intensity(stock) - Intensity(\text{sup})}{Intensity(stock)} \times 100\%$$

To confirm that the nanofibers were not just bound to the microparticle surface, 1 mg of microparticles were washed multiple times with water and the release of rhodamine-OVA-KFE8 in the washes was calculated against an equal weight of microparticles treated with 0.5 M EDTA (100% release). The stability of the composite microparticles in acidic environment of the gut was investigated by a dissolution test where the microparticles were exposed to simulated gastric fluid (pH 1.2) compared to PBS (pH 7.5) for 90 minutes. The release of rhodamine-OVA-KFE8 over time was calculated using fluorescence measurements compared against an equal weight of microparticles treated with 0.5 M EDTA (100% release). Morphology of the microparticles after exposure to simulated gastric fluid was determined using scanning electron microscopy as discussed below. The size distribution was obtained using confocal laser microscopy to first image the particles, followed by using ImageJ (NIH) to measure the diameter of the microparticles. 500 microparticles per batch were used to calculate the average diameter and size distribution range.

In vitro uptake of OVA-KFE8/$CaCO_3$ composite microparticles

To generate BMDCs, bone marrow was collected from the femurs of C57BL6 mice, suspended in RPMI-1640 medium (Invitrogen) supplemented with 10% heat-inactivated fetal bovine serum (HyClone), 1% penicillin-streptomycin, and 50 μM β-mercaptoethanol (Sigma Aldrich). Red blood cells were lysed using ACK buffer (Sigma Aldrich, MO) and cells were washed and re-suspended media supplemented with 50 ng/mL of granulocyte–macrophage colony-stimulating factor (GM-CSF). 10^6 cells/well were plated in six-well plates and cultured at 37°C for 7–9 days. Cells were fed on days 3, 5 and 7 with complete medium containing GM-CSF and on day 9, non-adherent cells were collected, washed and used for experiments. 50,000 cells/well were plated on cover slips in 6-well plates and primed with 50 ng/ml LPS for 18 hours and followed by 8-hour incubation with 100,000 composite microparticles (rhodamine-OVA-KFE loaded). The cover slips were gently removed, washed in media, and imaged using confocal microscopy (see below). To determine IL-1β production following microparticle uptake, culture media supernatant was collected and cytokine levels measured using mouse IL-1β ELISA Ready-SET-Go kit (eBioscience) as per protocols provided by the manufacturer. Cell surface markers Live/Dead (AmCyan), CD3 (PB), CD11b (PE), CD11c (PerCP-Cy5.5), CD80 (PE), CD86 (APC), and MHC-II (FITC) antibodies were purchased from BD Biosciences (San Jose, CA) and cell surface marker staining was performed according to standard protocol. Flow Cytometry was performed using a BD LSR Fortessa and FlowJo software (Tree Star, OR) was used to analyze data.

Ligated ileal loops and Immunohistochemistry

To investigate the uptake of OVA-KFE8/$CaCO_3$ composite microparticles by gut resident dendritic cells *in vivo*, 8-12 week old $CX3CR1^{gfp/gfp}$ reporter mice (transgenic mice whose $CX3CR1^{+}$ DCs express GFP) were fasted overnight and anesthetized by intraperitoneal injection of ketamine (100 mg/kg) and xylazine (20 mg/kg). After making a small abdominal incision, two 3-5 cm segments of the distal ileum each containing a Peyer's patch were ligated. The proximal loop was injected with PBS (~200 µl) and the distal loop with OVA-KFE8 nanofibers or OVA-KFE8/CaCO3 microparticles (8×10^6/mouse) suspended in a similar volume of PBS. Thirty minutes later, mice were euthanized by cervical dislocation and the loops excised and fixed in 4% PFA + 10% sucrose for 1 hour at 4 °C. Fixed tissue was then embedded in Tissue-Tek OCT medium (Sakura Finetek, CA), frozen in liquid nitrogen, and stored at -80 °C for processing. A subset of mice was orally gavaged with composite microparticles (8×10^6/mouse) and 2 h later mice were euthanized, MLNs were collected, and processed for immunohistochemistry.

Intestinal tissue or mesenteric lymph nodes were sectioned (10 µM) and rehydrated in PBS with calcium and magnesium at room temperature for 5 minutes and then fixed with 100 µL of 1% paraformaldehyde for 30 minutes at RT. The sections were then washed 4 times in PBS, incubated in blocking buffer (2.5% rat serum + 0.5 µg/ml Fc blocker in PBS) at RT for 30 min, and stained with M cell antibody (30 µg/ml, cat # NKM 16-2-4, Miltenyi Biotech) at RT for 60 min. Tissue sections were washed again 3 times in PBS followed by nuclear staining with 4′,6-diamidino-2-phenylindole (DAPI) (Invitrogen).

Microscopy

Peptide nanofibers were imaged using transmission electron microscopy and imaged on a JEM1400 TEM (JEOL) equipped with LaB_6 electron gun and digital cameras. Stock solutions of 1 mM peptides were allowed to fibrillize in water overnight at room temperature, diluted in PBS to 0.3 mM and applied to 300 mesh copper grids with carbon support film (Quantifoil). The grids were negatively stained with 2% uranyl acetate and images were viewed and recorded with an Ultrascan 1000 camera (Gatan). OVA-KFE8/$CaCO_3$ composite microparticles were imaged using a Nova NanoSEM 230 scanning electron microscope. Samples were sputtered with a 10 nm platinum-palladium coat to enhance the contrast and imaged using at an acceleration voltage of 7 kV. For confocal laser microscopy analysis, images were collected using a Zeiss LSM-510 META confocal microscope with 63× oil 1.4 NA objective and three different channels of emission with sequential acquisition. After excitation with the 364-nm, 488-nm, and 543-nm laser lines, emission was measured with a 385–470-nm filter, 505– 530-nm filter, and a 560–615-nm filter respectively. Confocal microscopy was conducted at the Optical Microscopy Core at UTMB.

Animals and immunizations

All experiments were conducted under protocols approved by the Institutional Animal Care and Use Committee at the University of Texas Medical Branch. Female mice (C57BL/6, 6-8 weeks old) were purchased from Taconic Farms and allowed to acclimate for a week prior to vaccinations. Oral vaccines were administered using a 22G gavage needle and mice were fasted

6 h prior to vaccination but given water *ad libitum*. OVA-KFE8/CaCO3 microparticles suspended in sterile PBS and OVA-KFE8 nanofibers were prepared for vaccination as described previously. Control mice received PBS or OVA peptide admixed with the gold standard mucosal adjuvant CTB. To ensure mice in all treatment groups recieved equivalent amounts of OVA, mice were gavaged orally on days 1, 2, and 3 with 400 nmol of OVA-KFE8 nanofibers (200 μL of 2 mM formulation) or 13.5×10^6 OVA-KFE8/$CaCO_3$ microparticles (200 μL of PBS) or 400 nmol of OVA admixed with 10 μg of CTB (200 μL of PBS). Mice were boosted with half the dose of all formulations on days 14 and 21 and sacrificed on day 35. To determine mucosal antibody responses, colon contents were collected, weighed and antibodies were extracted using ice-cold extraction buffer (1 ml PBS supplemented with 0.1 mg/ml trypsin inhibitor and 2 mM EDTA per 100 mg fecal pellet). The pellets were ground and a proportionate amount of extraction buffer was added to the pellets and incubated for 20 min on ice followed by centrifugation at 13,000 rpm for 15 min. 400 μL of extract supernatant was collected and mixed with 100 μL of glycerol and phenylmethylsulfonyl fluoride (100 mM) was added to the mixture prior to storage. For analysis of systemic antibody production, trunk blood was collected, serum extracted and stored at -80°C until use. To account for batch-to-batch variation in nanofiber formation and microparticle synthesis, mice were vaccinated with two different synthetic preparations of nanofibers or microparticles with 3-4 mice per group per experiment.

Antibody responses and isotypes

High-binding ELISA plates (eBioscience, CA) were coated with 20 μg/mL of OVA peptide in PBS overnight at 4°C and blocked with 200 μL of 0.5% BSA in PBST (0.5% Tween-20 in PBS) for 1 h. Serum and fecal extract were diluted 1:100 in PBST dilutions and applied to

the plates (100 μL/well) for 1 h at room temperature followed by peroxidase-conjugated goat anti-mouse IgG (H+L) (Jackson Immuno Research, PA) (1:5000 in 0.5% BSA-PBST, 100 μL/well). Plates were developed using TMB substrate (100 μL/well, eBioscience, CA), the reaction stopped using 50 μl of 1 M phosphoric acid, and absorbance measured at 450 nm. Absorbance values of PBS (no antigen) coated wells were subtracted to account for background. Antibody isotypes were determined using a mouse monoclonal antibody kit (Sigma, MO) with secondary goat anti-mouse IgG1, IgG2a, IgG2b, IgG3, IgM, and IgA.

Statistical analysis

All the experimental data were plotted using GraphPad Prism software and represented as mean ± SEM. Grubb's test was used to identify any statistical outliers and analysis was performed by ANOVA with Tukey's post hoc test. Significance was assigned at p values <0.05.

Acknowledgements

This study was supported by funds from the Sealy Center for Vaccine Development, and the Department of Pharmacology and Toxicology, UTMB (J.S.R). TEM studies were conducted at the Sealy Center for Structural Biology Cryo-electron Microscopy core lab and we thank Dr. Misha Sherman and Michael Woodson for assistance with imaging. Flow cytometry was conducted at the Flow Cytometry and Cell Sorting Facility at UTMB and we thank Mark Griffin for his expertise. We also thank Dr. Lars Eckmann, University of California San Diego, for his kind gift of CX3CR1$^{gfp/gfp}$ mice. We gratefully acknowledge Dr. Cheryl Lichti and Heather Landers for assistance with editing the manuscript.

Figure Legends

Figure 1. (a) Schematic depicting OVA-KFE8/$CaCO_3$ composite microparticle synthesis. OVA-KFE8 nanofibers (TEM image) were dissolved in 0.33 M $CaCl_2$ to which 0.33 M Na_2CO_3 solution was added under stirring. Precipitation of $CaCO_3$ resulted in encapsulation of OVA-KFE8 nanofibers within the $CaCO_3$ matrix (SEM image). (b) Confocal microscopy images of OVA-KFE8 nanofibers and OVA-KFE8/$CaCO_3$ composite microparticles showing conversion from fibrous aggregates into discrete spherical microparticles.

Figure 2. (a) Encapsulation efficiency of OVA-KFE8 nanofibers in $CaCO_3$ microparticles as a function of peptide nanofiber concentration. Highest nanofiber encapsulation ~72% was observed at 2 mM peptide concentration. (b) Figure showing loss of surface bound nanofibers from composite microparticles after serial washes. To calculate percentage of nanofibers released during serial washes, microparticles were dissolved in EDTA (100% release) and fluorescence intensity of supernatants was measured. Data indicated that ~8% of nanofibers are washed out and not bound within the microparticle core. *$p<0.05$ by ANOVA using Tukey post-hoc test.

Figure 3. (a) SEM micrographs of intact control $CaCO_3$ microparticles depicting spherical morphology and cross section showing a highly porous interior. (b) Composite microparticles are also spherical but have a denser surface and core suggesting nanofiber loading within the particle.

(c) Size distribution of control $CaCO_3$ microparticles and (d) composite microparticles. Control microparticles had an average diameter of 3.5 μm whereas composite microparticles had an average diameter of 2.2 μm. Data shown is an average of 500 microparticles for each group.

Figure 4. (a) Stability of OVA-KFE8/$CaCO_3$ composite microparticles in simulated gastric fluid (SGF). Scanning electron micrographs of composite microparticles (a) before and (b) after 90 min of incubation in SGF. Composite microparticles displayed increased porosity following treatment with SGF but retained their spherical morphology. (c) Data showing release of OVA-KFE8 nanofibers in SGF over time. Fluorescence intensity measurements indicated that following 90 min of incubation ≈20% of the encapsulated nanofibers fibers were released.

Figure 5. Treatment of BMDCs with composite microparticles leads to DC maturation and production of pro-inflammatory cytokines. (a) Flow cytometry histograms of DC maturation markers (a) CD80 and (b) CD86 after 8 h incubation with composite microparticles showing significantly higher levels of co-stimulatory markers in DCs treated with microparticles compared to untreated or DCs treated with OVA-KFE8 nanofibers. (c) Confocal microscopy image showing phagocytosis of composite microparticles by BMDCs. (d) Treatment of BMDCs with composite microparticles leads to the production of cytokine IL-1β and significantly higher levels of IL-1β were detected in BMDC cultures treated with composite microparticles compared to OVA-KFE8 nanofibers or controls. *$p<0.05$ by ANOVA using Tukey post-hoc test.

Figure 6. Uptake of composite microparticles *in vivo* assessed by ligated ileal loop assays or oral gavage of composite microparticles in transgenic CX3CR1$^{gfp/gfp}$ mice using confocal microscopy. (a) Images of intestinal villi showing composite microparticles within the lamina propria co-

localized CX3CR1^{+} DCs. Microparticles in the intestinal lumen at the mucus barrier can be seen. (b) Uptake of composite microparticles by M cells in mouse PPs. M cells were stained using an anti-M cell antibody and data shows co-localization of composite microparticles with M cells. (c) MLNs are a major inductive site as evidenced by the co-localization of CX3CR1^{+} DCs and composite microparticles within MLNs of CX3CR1$^{gfp/gfp}$ mice orally gavaged with composite microparticles. Nuclei were stained with DAPI (blue), microparticles (red), CX3CR1^{+} DCs or M cell antibody (green). Data are representative of images collected from 3 mice per group.

Figure 7. Oral vaccination with composite microparticles induces robust mucosal antibody responses. (a) Total mucosal anti-OVA antibody titers (H+L) measured from fecal extracts of mice vaccinated orally with OVA-KFE8/$CaCO_3$ composite microparticles or controls. Significantly higher mucosal antibody production was observed in mice vaccinated with composite microparticles compared to PBS, OVA-KFE8 nanofibers, or OVA-CTB vaccinated mice. (b) Systemic antibody responses measured using sera from mice vaccinated orally with composite microparticles or controls. Significantly higher antibody responses were detected in mice vaccinated with composite microparticles compared to PBS or OVA-KFE8 nanofibers. Data is cumulative of two independent experiments (n = 3-4 mice per group per experiment). *$p<0.05$ by ANOVA using Tukey post-hoc test.

Figure 8. Mucosal antibody isotypes in fecal extracts of mice immunized orally with composite microparticles or controls. (a) Significantly higher levels of IgA isotype were detected in composite microparticle vaccinated mice compared to controls whereas (b) IgG1 was significantly higher in OVA-CTB vaccinated mice. Isotypes (c) IgG3 and (d) IgM were also

detected in mice vaccinated with composite microparticles and were significantly higher than PBS controls. Data is cumulative of three independent experiments (n = 3-4 mice per group per experiment). *$p < 0.05$ by ANOVA using Tukey post-hoc test.

Figures

Figure 1.

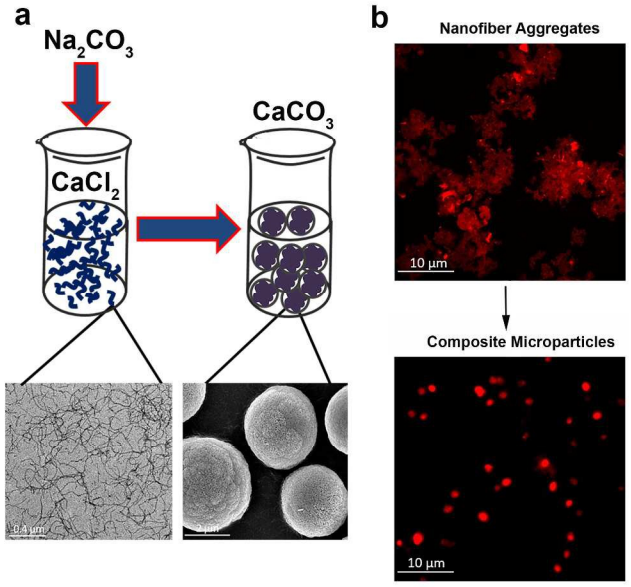

Figure 2

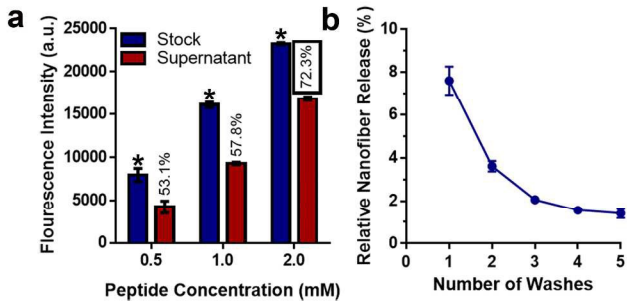

Figure 3

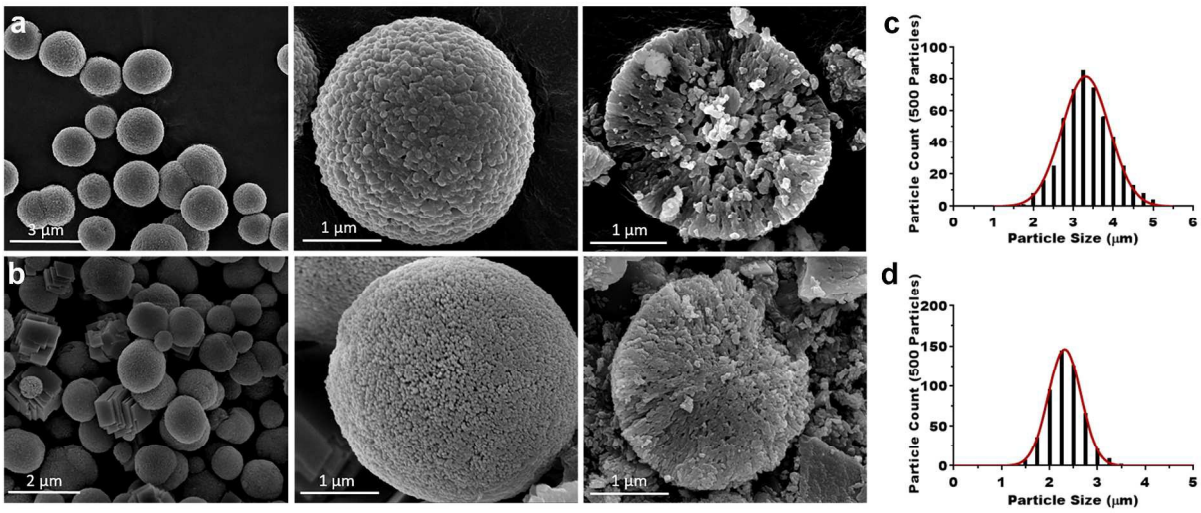

Figure 4

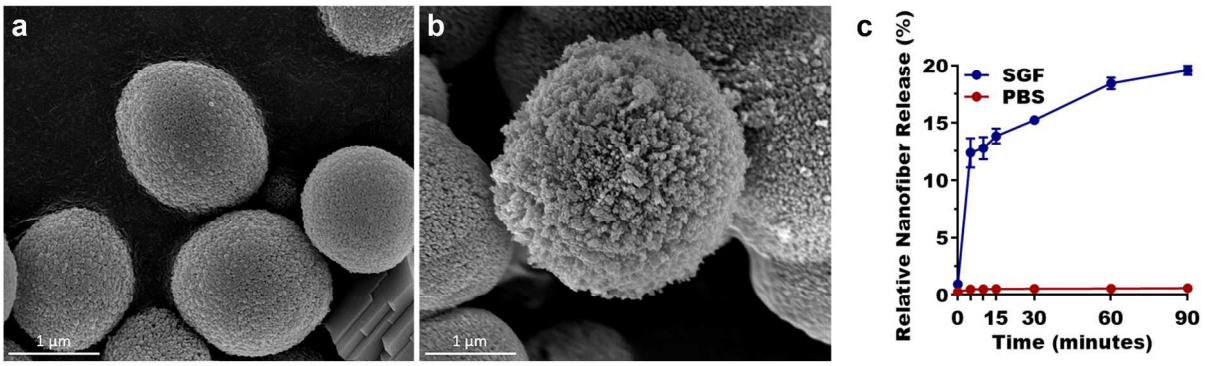

Figure 5

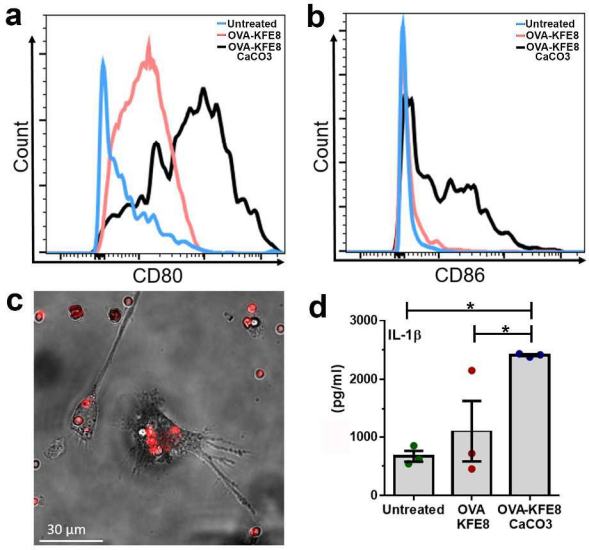

Figure 6

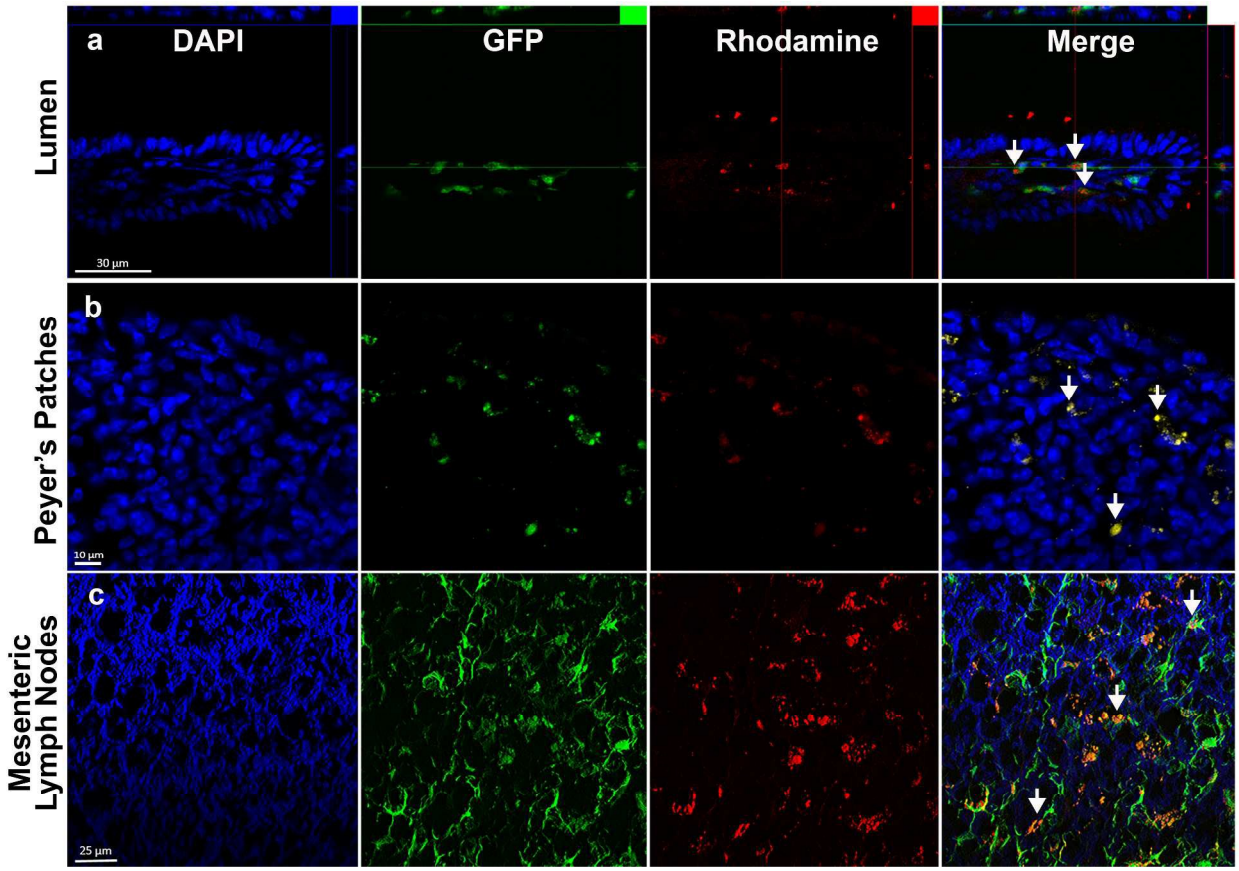

Figure 7.

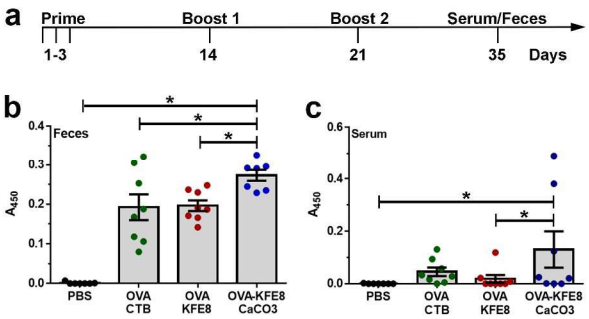

Figure 8

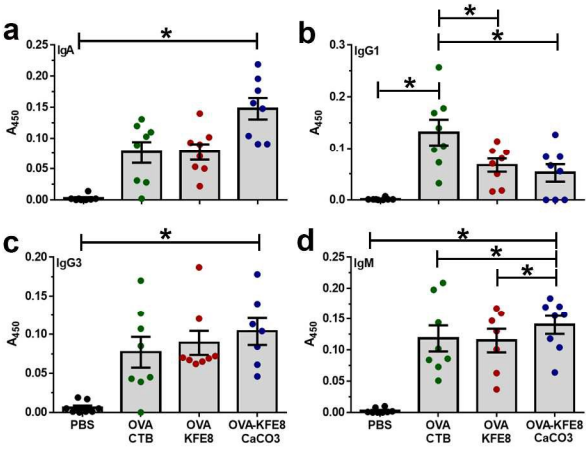

References

1. K. A. Woodrow, K. M. Bennett and D. D. Lo, Annu Rev Biomed Eng, 2012, 14, 17-46.
2. M. R. Neutra and P. A. Kozlowski, *Nat Rev Immunol*, 2006, **6**, 148-158.
3. J. Pépin, C. N. Abou Chakra, E. Pépin, V. Nault and L. Valiquette, *PLoS ONE*, 2014, **9**, e99677.
4. Y. Fujkuyama, D. Tokuhara, K. Kataoka, R. S. Gilbert, J. R. McGhee, Y. Yuki, H. Kiyono and K. Fujihashi, *Expert Rev Vaccines*, 2012, **11**, 367-379.
5. Q. Zhu and J. A. Berzofsky, *Gut Microbes*, 2013, **4**, 246-252.
6. M. Laassri, K. Lottenbach, R. Belshe, M. Rennels, S. Plotkin and K. Chumakov, *J Infect Dis* 2006, **193**, 1344-1349.
7. M. Black, A. Trent, M. Tirrell and C. Olive, *Expert Rev Vaccines*, 2010, **9**, 157-173.
8. D. T. O'Hagan and E. De Gregorio, *Drug Discov Today*, 2009, **14**, 541-551.
9. J. C. Aguilar and E. G. Rodriguez, *Vaccine*, 2007, **25**, 3752-3762.
10. D. J. Lewis, Z. Huo, S. Barnett, I. Kromann, R. Giemza, E. Galiza, M. Woodrow, B. Thierry-Carstensen, P. Andersen, D. Novicki, G. Del Giudice and R. Rappuoli, *PLoS One*, 2009, **4**, e6999.
11. F. W. van Ginkel, R. J. Jackson, N. Yoshino, Y. Hagiwara, D. J. Metzger, T. D. Connell, H. L. Vu, M. Martin, K. Fujihashi and J. R. McGhee, *Infect Immun*, 2005, **73**, 6892-6902.
12. L. B. Lawson, E. B. Norton and J. D. Clements, *Curr Opin Immunol*, 2011, **23**, 414-420.
13. H.-J. Choi, C. F. Ebersbacher, M.-C. Kim, S.-M. Kang and C. D. Montemagno, *PLoS ONE*, 2013, **8**, e66316.
14. B. Devriendt, B. G. De Geest and E. Cox, *Expert Opin Drug Deliv*, 2011, **8**, 467-483.
15. N. A. Mabbott, D. S. Donaldson, H. Ohno, I. R. Williams and A. Mahajan, *Mucosal Immunol*, 2013, **6**, 666-677.
16. S. H. Kim, D. I. Jung, I. Y. Yang, S. H. Jang, J. Kim, T. T. Truong, T. V. Pham, N. U. Truong, K. Y. Lee and Y. S. Jang, *Int Immunol*, 2013, **25**, 623-632.
17. L. M. Ensign, R. Cone and J. Hanes, *Adv Drug Deliv Rev*, 2012, **64**, 557-570.
18. E. A. McNeela and E. C. Lavelle, *Curr Top Microbiol Immunol*, 2012, **354**, 75-99.
19. T. Jiang, B. Singh, H. S. Li, Y. K. Kim, S. K. Kang, J. W. Nah, Y. J. Choi and C. S. Cho, *Biomaterials*, 2014, **35**, 2365-2373.
20. J. M. de Barros, T. Scherer, D. Charalampopoulos, V. V. Khutoryanskiy and A. D. Edwards, *J Pharm Sci*, 2014, **103**, 2022-2032.
21. I. M. van der Lubben, J. C. Verhoef, G. Borchard and H. E. Junginger, *Adv Drug Deliv Rev*, 2001, **52**, 139-144.
22. B. Shrestha and J. P. Rath, *IET Nanobiotechnol*, 2014, **8**, 201-207.

23. R. De Smet, T. Demoor, S. Verschuere, M. Dullaers, G. R. Ostroff, G. Leclercq, L. Allais, C. Pilette, M. Dierendonck, B. G. De Geest and C. A. Cuvelier, *J Control Release*, 2013, **172**, 671-678.
24. N. Wang, T. Wang, M. Zhang, R. Chen, R. Niu and Y. Deng, *European Journal of Pharmaceutics and Biopharmaceutics*, 2014, **88**, 194-206.
25. K. Dixit, R. B. Athawale and S. Singh, *J Microencapsul*, 2015, **32**, 107-122.
26. V. Pavot, N. Rochereau, C. Genin, B. Verrier and S. Paul, *Vaccine*, 2012, **30**, 142-154.
27. J. S. Rudra, Y. F. Tian, J. P. Jung and J. H. Collier, *Proc Natl Acad Sci U S A*, 2010, **107**, 622-627.
28. J. S. Rudra, T. Sun, K. C. Bird, M. D. Daniels, J. Z. Gasiorowski, A. S. Chong and J. H. Collier, *ACS Nano*, 2012, **6**, 1557-1564.
29. J. S. Rudra, S. Mishra, A. S. Chong, R. A. Mitchell, E. H. Nardin, V. Nussenzweig and J. H. Collier, *Biomaterials*, 2012, **33**, 6476-6484.
30. C. B. Chesson, E. J. Huelsmann, A. T. Lacek, F. J. Kohlhapp, M. F. Webb, A. Nabatiyan, A. Zloza and J. S. Rudra, *Vaccine*, 2014, **32**, 1174-1180.
31. G. A. Hudalla, J. A. Modica, Y. F. Tian, J. S. Rudra, A. S. Chong, T. Sun, M. Mrksich and J. H. Collier, *Adv Healthc Mater*, 2013, **2**, 1114-1119.
32. Z. H. Huang, L. Shi, J. W. Ma, Z. Y. Sun, H. Cai, Y. X. Chen, Y. F. Zhao and Y. M. Li, *J Am Chem Soc*, 2012, **134**, 8730-8733.
33. J. Wang, J.-S. Chen, J.-Y. Zong, D. Zhao, F. Li, R.-X. Zhuo and S.-X. Cheng, *J Phys Chem C*, 2010, **114**, 18940-18945.
34. D. Volodkin, *Adv Colloid Interface Sci*, 2014, **207**, 306-324
35. B. V. Parakhonskiy, A. Haase and R. Antolini, *Angew Chem Int Ed*, 2012, **51**, 1195-1197.
36. A. I. Petrov, D. V. Volodkin and G. B. Sukhorukov, *Biotechnol Prog*, 2005, **21**, 918-925.
37. D. B. Trushina, T. V. Bukreeva, M. V. Kovalchuk and M. N. Antipina, *Mater Sci Eng C Mater Biol Appl*, 2014, **45**, 644-658.
38. E. M. Flaten, M. Seiersten, and J. P. Andreassen, *J. Cryst. Growth*, 2009, **311**, 3553-3538.
39. R. De Smet, S. Verschuere, L. Allais, G. Leclercq, M. Dierendonck, B. G. De Geest, I. Van Driessche, T. Demoor and C. A. Cuvelier, *Biomacromolecules*, 2014, **15**, 2301-2309.
40. J.J. Chen, R.R. Pompano, F.W. Santiago, L. Maillat, R. Sciammas, T. Sun, H. Han, D. J. Topham, A.S. Chong, and J.H. Collier, *Biomaterials*, 2014, **34**, 8776-8785.
41. J. T. Merrill, *Clinical Immunology*, 2013, **148**, 369-375.
42. S. Frosali, D. Pagliari, G. Gambassi, R. Landolfi, F. Pandolfi and R. Cianci, *J Immunol Res*, 2015, **2015**, 12.
43. S. Krishna and L. S. Miller, *Semin Immunopathol*, 2012, **34**, 261-280.
44. T. T. Lina, I. V. Pinchuk, J. House, Y. Yamaoka, D. Y. Graham, E. J. Beswick and V. E. Reyes, *J Immunol*, 2013, **191**, 3838-3846.
45. Y. Kurashima, Y. Goto and H. Kiyono, *Eur J Immunol*, 2013, **43**, 3108-3115.
46. M. Rescigno, *Immunity*, 2006, **24**, 508-510.
47. J. H. Niess, S. Brand, X. Gu, L. Landsman, S. Jung, B. A. McCormick, J. M. Vyas, M. Boes, H. L. Ploegh, J. G. Fox, D. R. Littman and H. C. Reinecker, *Science*, 2005, **307**, 254-258.

48. M. Yamamoto, P. Rennert, J. R. McGhee, M. N. Kweon, S. Yamamoto, T. Dohi, S. Otake, H. Bluethmann, K. Fujihashi and H. Kiyono, *J Immunol*, 2000, **164**, 5184-5191.
49. A. Cerutti, K. Chen and A. Chorny, *Annu Rev Immunol*, 2011, **29**, 273-293.
50. S. K. Lai, D. E. O'Hanlon, S. Harrold, S. T. Man, Y. Y. Wang, R. Cone and J. Hanes, *Proc Natl Acad Sci U S A*, 2007, **104**, 1482-1487.
51. T. E. Rajapaksa, K. M. Bennett, M. Hamer, C. Lytle, V. G. J. Rodgers and D. D. Lo, *J Biol Chem*, 2010, **285**, 23739-23746.
52. R. Appavu, C.B. Chesson, A. Koyfman, J.D. Snook, F. Kholhapp, A. Zloza, J.S. Rudra, *ACS Biomat Sci Eng*, 2015, **1**, 601-609
53. Y. Boyjoo, V. K. Pareek and J. Liu, *J Mater Chem A*, 2014, **2**, 14270-14288.

Graphical Abstract